Journal of Solid State Chemistry **162,** 158–167 (2001)
doi:10.1006/jssc.2001.9206, available online at http://www.idealibrary.com on IDEAL®

$Th_3Co_3Sb_4$: A New Room Temperature Magnet

Sandrine Sportouch and Mercouri G. Kanatzidis[1]

Department of Chemistry, Michigan State University, East Lansing, Michigan 48824

Received November 9, 2000; in revised form March 29, 2001; accepted April 12, 2001; published online June 11, 2001

IN HONOR OF PROFESSOR PAUL HAGENMULLER ON THE OCCASION OF HIS 80TH BIRTHDAY

The new ternary compound $Th_3Co_3Sb_4$ was synthesized by arc melting. The compound crystallizes in the cubic space group *I*-43*d* (No. 220) with $a = 9.572(2)$ Å and adopts the $Y_3Au_3Sb_4$ structure, which is a filled version of the Th_3P_4 structure type. The crystal structure was solved and refined with single-crystal X-ray diffraction. Final $R1/Rw2 = 1.52/3.73\%$. $Th_3Co_3Sb_4$ is a metallic ferromagnet at room temperature. Electrical conductivity and thermoelectric power measurements show metallic behavior, which is also predicted by the electronic band structure calculations. © 2001 Elsevier Science

INTRODUCTION

Since the discovery of $Y_3Au_3Sb_4$ more than 20 years ago (1) a long series of compounds with the general formula $R_3M_3X_4$ was synthesized. R, mainly, corresponds to a rare earth element, M to a transition metal from groups 9 to 11, and X to a pnictide or stannide element: more specifically to As, Sb, Bi, and Sn. However, compounds with group 4 transition elements as well as actinides (2) also exist. These compounds have attracted attention due to the unusual transport and magnetic properties. For example, the mixed-valent $Ce_3Pt_3Sb_4$ (3–5), and the $R_3Au_3Sb_4$ (R = Ce, Nd, Sm, Gd, Ho) (4, 6), $U_3M_3Sb_4$ (M = Ni, Pd, Pt and Cu) (7–11), and $R_3Cu_3Sb_4$ (R = Y, La, Ce, Pr, Nd, Sm, Gd, Tb, Dy, Ho, Er) (12) are narrow gap semiconductors. The $Pr_3Pt_3Sb_4$ (3) and $Ce_3Pt_3Bi_4$ (13–15) exhibit metallic and Kondo insulating behaviors, respectively. It is interesting to note here that the "so-called" intermetallic Kondo insulator materials (16) are characterized by both a rare earth or actinide formal oxidation state of +4 and semiconducting behavior. $U_3Co_3Sb_4$ (9), $U_3Cu_3Sb_4$ (7, 11, 17), and $Ce_3Cu_3Sb_4$ (18) are representative of ferromagnetic materials ($T_C = 35$, 88, and 10 K, respectively), whereas $Sm_3Au_3Sb_4$ (4), $Gd_3Au_3Sb_4$ (4), and $Gd_3Cu_3Sb_4$ (12, 18) are reported to be antiferromagnets ($T_N = 2$, 11, and 12 K, respectively). By comparison the $R_3Cu_3Sb_4$ (R = La, Y) members are diamagnetic (12). The $U_3M_3Sn_4$ members (M = Ni, Pt, Cu, Au) (7, 11, 17) show heavy-fermion behavior, and generally, such systems have a metallic ground state that is either paramagnetic, antiferromagnetic, or superconducting (15).

In addition to the properties described above, recent interest in thermoelectric properties has stimulated research on complex crystal structures with heavy elements, and Kondo or heavy fermion characteristics in order to achieve low-thermal conductivity and high thermopower (19–22). Only a few members contain thorium; these include $Th_3Ni_3Sn_4$, which exhibits superconducting behavior (23), and $Th_3Ni_3Sb_4$ (24).

Here we describe $Th_3Co_3Sb_4$ and report its crystal structure and its electrical and magnetic properties. Moreover, the role of Co in the bonding stability and in the properties of the compound was explored with electronic band structure calculations.

EXPERIMENTAL

Synthesis

The following chemicals were used as obtained: thorium, 99.8%, −100 mesh, Cerac, Milwaukee, WI; cobalt powder, 99.9%, −100 mesh, Aldrich Chemical Co., Inc., Milwaukee, WI. Antimony (shot form, 99.9%, Noranda Advanced Materials, Quebec Canada) was ground into a fine powder before use. All manipulations were carried out under a dry nitrogen atmosphere in a glove box.

Method 1. A mixture of 0.8000 g (3.448 mmol) of Th, 0.2032 g (3.448 mmol) of Co, and 0.4197 g (3.448 mmol) of Sb was pressed into a pellet inside a glove box. The pellets were then arc melted under inert atmosphere composed of Ar/He gas mixture. The sample was flipped over and melted again, and this operation was carried out three times to ensure a well-homogenized sample. The arc-melted sample was then flame-sealed in a silica tube under vacuum (10^{-5} Torr). The ingot was annealed at 900°C for five days and cooled to room temperature at a rate of −35°C/h. The final product

[1]To whom correspondence should be addressed.

0022-4596/01 $35.00

corresponds to the pure $Th_3Co_3Sb_4$ phase surrounded by a ThO_2 crust. The product was isolated from the crust by immersion in a 30% HCl solution (by volume) for 12 h. The purity of the final product was confirmed by EDS analysis and by comparison of the experimental X-ray diffraction pattern to a theoretical pattern calculated from the refined single-crystal data.

Method 2. A mixture of 0.4570 g (1.969 mmol) of Th, 0.1160 g (1.969 mmol) of Co, and 0.3197 g (2.626 mmol) of Sb was loaded into a capped graphite tube, placed in an induction furnace, and heated under argon atmosphere for 2 min using a power of 0.75 kW. The temperature reached was about 1450°C. $Th_3Co_3Sb_4$ was obtained in pure form.

EDS analysis. Semi-quantitative microprobe analysis of the compounds were carefully performed with a JEOL JSM-6400V scanning electron microscope (SEM) equipped with a Noran Vantage energy dispersive spectroscopy (EDS) detector. Data were acquired by using an accelerating voltage of 25 kV and a 40-s accumulation time. The analyses of various pieces from both synthetic methods agree with the $Th_3Co_3Sb_4$ formula. No phase heterogeneity was detected.

Differential thermal analysis (*DTA*). Differential thermal analysis (DTA) was performed with a computer-controlled Shimadzu DTA-50 thermal analyzer. Approximately 32 mg of the sample, in a ground form, was sealed in a silica ampoule under vacuum. A silica ampoule containing alumina of equal mass was sealed and placed on the reference side of the detector. The sample was heated to 1000°C at 10°C/min, kept there for 5 min, and then cooled at a rate of 10°C/min to 50°C, followed by rapid cooling to room temperature. The stability and reproducibility of the samples was monitored by running multiple heating and cooling cycles. Residues of the DTA experiments were examined by powder X-ray diffraction.

X-ray crystallography. Powder X-ray diffractograms were recorded on a Rigaku Rotaflex powder X-ray diffractometer with Cu$K\alpha$ radiation operating at 45 kV and 100 mA. The diffractometer was equipped with a monochromator placed between the sample and the detector (this configuration eliminates the strong Co fluorescence). The data were collected at a rate of 0.5°/min.

A single crystal of the title compound (crystal size: $0.05 \times 0.05 \times 0.04\,mm^3$), obtained from method 1, was selected and mounted on the tip of a glass fiber. Crystallographic data were collected on a Siemens SMART Platform CCD diffractometer using a graphite-monochromatized Mo$K\alpha$ ($\lambda = 0.71073$ Å) radiation over a hemisphere of reciprocal space. The individual frames were measured with an ω rotation of 0.3° and an acquisition time of 45 s per frame. The SMART software (25) was used for the data acquisition and SAINT (26) for data extraction and reduction. An empirical absorption correction, using the program SADABS (27), was applied to the data. The complete data collection parameters and details of the structure solution and refinement are given in Table 1.

TABLE 1
Crystallographic Data for $Th_3Co_3Sb_4$

Formula weight	1359.91
Temperature	293(2) K
Space group	I-43d (#220)
Unit cell dimensions	a = 9.572(2) Å
$V = 877.1(3)$ Å^3	
$Z = 4$	
D_{calc} (g/cm^3)	10.299
Absorption coefficient (mm^{-1})	68.186
$F(000)$	2220
Crystal size (mm^3)	$0.05 \times 0.05 \times 0.04$
Radiation	Mo$K\alpha$ ($\lambda = 0.71073$ Å)
2Θ range (°)	5.22–28.58
Index ranges	$-12 \le h \le 12$
	$-12 \le k \le 12$
	$-12 \le l \le 12$
Reflections collected	4416
Unique reflections	185 [$R_{(int)} = 0.0623$]
G.O.F. on F^2	1.150
$R1/wR2$ [$I > 2\sigma(I)$]	0.0152/0.0373
$R1$/w$R2$(all data)	0.0183/0.0383
Max. peak and hole (e.Å^{-3})	0.724/−1.124
Extinction coefficient	0.00034(7)

Structure solution and refinement of the compound were performed with the SHELXTL package of crystallographic programs (28). The structure was refined anisotropically in the I-43d space group. Fractional atomic coordinates and equivalent isotropic displacement parameters (U_{eq}) are given in Table 2, and the anisotropic temperature factors and bond parameters are reported in Tables 3 and 4, respectively.

Magnetic susceptibility. The magnetic response of the title compound was measured over the range 2–400 K using a MPMS Quantum Design SQUID magnetometer. A polycrystalline sample was ground to a fine powder and loaded into PVC containers. The temperature-dependent magnetic

TABLE 2
Atomic Coordinates and Equivalent Isotropic Displacement Parameters (Å^2×10^3) for $Th_3Co_3Sb_4$

Atoms	Wyckoff position	x	y	z	U(eq)	Occ.
Th	12a	0	$\frac{3}{4}$	$\frac{1}{8}$	9(1)	1
Sb	16c	−0.0790(1)	0.4211(1)	0.0790(1)	8(1)	1
Co	12b	$\frac{1}{8}$	$\frac{1}{2}$	$\frac{1}{4}$	14(1)	1

Note. U(eq) is defined as one-third of the trace of the orthogonalized U_{ij} tensor.

TABLE 3
Anisotropic Displacement Parameters (Å²×10³) for $Th_3Co_3Sb_4$

Atoms	U_{11}	U_{22}	U_{33}	U_{23}	U_{13}	U_{12}
Th	8(1)	8(1)	11(1)	0	0	0
Sb	8(1)	8(1)	8(1)	−1(1)	−1(1)	1(1)
Co	15(1)	14(1)	14(1)	0	0	0

Note. The anisotropic displacement factor exponent takes the form $-2\pi^3[h^2 a^{*2} U_{11} + \cdots + 2h\,k\,a^* b^* U_{12}]$.

susceptibility studies were performed at 1000 G. The diamagnetic contribution of every ion to the molar susceptibility (χ_m) was corrected according to Selwood (29). Magnetization as a function of magnetic field was measured at 2 and 300 K. The magnetic property found in the material raised concerns for the possibility of Co metal impurity in the samples. The following experiments were conducted to probe for Co metal. The presumed $Th_3Co_3Sb_4$ product was ground to powder and soaked in 30% HCl solution to dissolve any possible transition metal impurities. The powder suspension was even sonicated for 12 h in aqueous 30% HCl solution and isolated by filtration afterward. The reported magnetic data are on such treated material. Material not treated with HCl solution gave a similar magnetic response. Powder X-ray diffraction showed no evidence of the Co metal. Energy dispersive elemental analysis performed under high magnification using a scanning electron microscope showed relatively uniform Th/Co/Sb ratios. Furthermore, arc-melted samples that were not annealed were polyphasic and often were not magnetic. Subsequent annealing of these samples gave good purity product (as judged by X-ray diffraction) and ferromagnetic behavior. We believe it is unlikely that the Co metal was absent in the preannealed samples but was generated in the annealing

TABLE 4
Selected Bond Lengths (Å) and Angles (°) for $Th_3Co_3Sb_4$

Th	−4 Co	2.9309(5)		Sb	−3 Co	2.6577(5)
	−4 Sb	3.2680(8)			−3 Th	3.2680(8)
	−4 Sb	3.3590(9)			−3 Th	3.3590(9)
Co	−4 Sb	2.6576(5)				
	−4 Th	2.9309(6)				
Co–Th–Co		99.6	(×4)	Co–Sb–Co		114.764(14)	(×3)
		131.8	(×2)				
				Co–Sb–Th		58.202(9)	(×6)
Co–Th–Sb		50.415(2)	(×8)			128.82(3)	(×3)
		138.363(11)	(×4)			56.878(7)	(×3)
		121.808(12)	(×4)			104.799(10)	(×2)
		49.414(11)	(×4)			104.800(10)	(×1)
		136.646(10)	(×4)			137.44(2)	(×3)
		87.807(8)	(×8)				
				Th–Sb–Th		86.47(2)	(×3)
Sb–Th–Sb		91.043(3)	(×2)			85.0	(×3)
		164.49(2)	(×1)			107.7	(×3)
						162.929(3)	(×3)
Sb–Th–Sb		164.50(2)	(×1)			83.58(2)	(×3)
		91.043(3)	(×2)				
		89.44(2)	(×4)	Sb–Co–Sb		85.46(2)	(×2)
		65.929(10)	(×4)			122.655(14)	(×4)
		129.457(11)	(×4)				
		77.4	(×4)	Sb–Co–Th		73.71(2)	(×4)
		64.941(2)	(×2)			71.383(11)	(×8)
		135.380(1)	(×4)			156.781(11)	(×4)
				Th–Co–Th		131.8	(×1)
						99.6	(×4)

TABLE 5
Exponents and Parameters Used in the Extended Hückel Calculations

Atoms	Orbitals	H_{ii}(eV)	ζ_1	c_1	ζ_2	c_2	Ref.
Th	7*s*	−5.39	1.834	1.0			32, 34
	7*p*	−5.39	1.834	1.0			
	6*d*	−10.11	2.461	0.7612	1.165	0.4071	
	5*f*	−9.64	4.477	0.7682	1.837	0.4267	
Co	4*s*	−9.21	2.0	1.0			32, 33
	4*p*	−5.29	2.0	1.0			
	3*d*	−13.18	5.55	0.568	2.10	0.606	
Sb	5*s*	−18.8	2.323	1.0			32, 35
	5*p*	−11.7	1.999	1.0			

Note. The contraction coefficients used in the double-ζ expansion are c_1 and c_2.

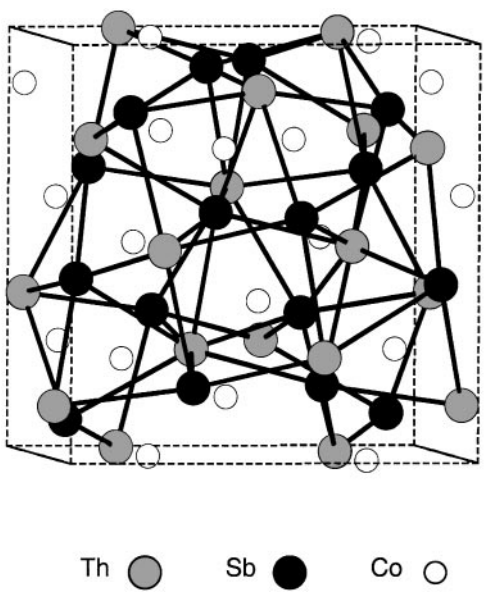

FIG. 1. The cubic crystal structure of $Th_3Co_3Sb_4$. Note that Co bonds were removed for clarity to highlight the Th_3Sb_4 framework.

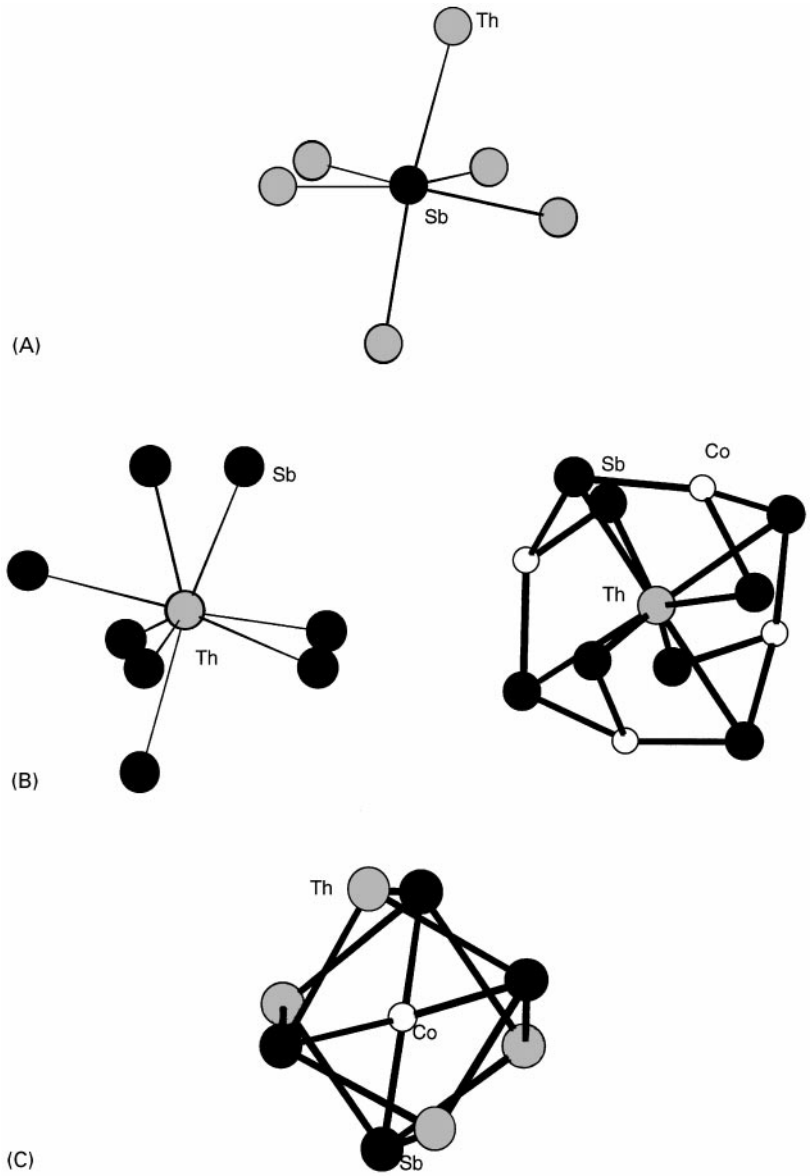

FIG. 2. Coordination environments of individual atoms in $Th_3Co_3Sb_4$.

step. In addition the saturation magnetization value observed was reproducible as would be expected from a pure phase.

Transport property measurements. Measurements of the thermopower were carried out over a temperature range from 300 to 570 K on polycrystalline compactions, using a programmable Seebeck controller SB100 from MMR Technologies, Inc. Constantan wire of 0.002″ thickness was chosen as reference, and both sample and reference were held in place with a conductive silver paste. Several runs were performed in order to assure reproducibility and accuracy of the measurements.

Room temperature conductivity measurement was performed using a four-probe homemade instrument. The system was calibrated using a Bi_2Te_3 block as a reference with a known conductivity value. This measurement is strongly shape dependent. Consequently, the value obtained is only indicative and not highly accurate.

Electronic band structure. The thorium atoms in $Th_3Co_3Sb_4$ are expected to have an empty $5f$ shell. The $5f$ orbitals are less localized and contracted than the $4f$ orbitals, and therefore a description of the $5f$ electron interactions is much more difficult. It is only after americium or curium that the $5f$ orbitals are sufficiently contracted to allow for a localized description. Therefore a strong mixing between the valence orbitals belonging to the rare earth ($5f$, $6d$, $7s$) element and those of the surrounding atoms is

expected. Consequently, the 5*f* orbitals were included in the electronic band structure calculations in order to obtain a more representative picture of the electronic band structure of $Th_3Co_3Sb_4$. Furthermore, insights about the influence of the 5*f* orbitals on the material's physical properties were sought by comparison of both the $Th_3Co_3Sb_4$ and Th_3Sb_4 band structures. The electronic band structure calculations were performed with the CAESAR 1.0 program package (30, 31). The atomic orbital parameters, i.e., energies and exponents, used in the Slater-type wave functions were chosen from one of the three data bases available in the CAESAR package and are given in Table 5 (32–35). The nondiagonal Hamiltonian matrix elements were computed with the modified Wolfsberg–Helmohtz formula (36).

RESULTS AND DISCUSSION

Synthesis and Thermal Properties

$Th_3Co_3Sb_4$ was synthesized by direct combination of the elements in an induction furnace at 1450°C. It can also be prepared with arc-melting followed by an annealing step at 900°C; however, an equimolar mixture is required to compensate for certain element evaporation. Surprisingly, the latter synthetic method gives an almost pure phase with only a small amount of thorium oxide (ThO_2) and no trace of unreacted elements such as Th or Co. The arc-melting method tends to give well-formed tiny single crystals, whereas the RF induction method produces polycrystalline chunks. On the other hand, no oxide phase is generated by induction heating and consequently no washing with HCl is required. DTA measurements show that $Th_3Co_3Sb_4$ does not melt up to 1000°C. X-ray diffraction after the DTA experiments confirmed that no phase transformation took place. However, a sintering phenomenon, which was responsible for transforming the initial powder sample into a solid chunk, occurred.

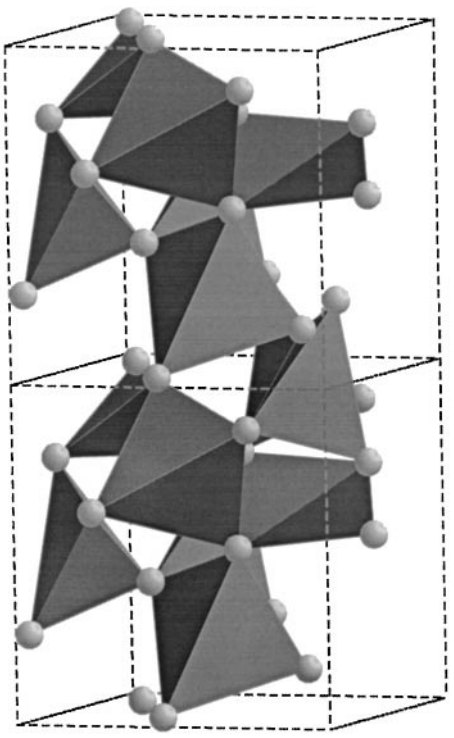

FIG. 3. The 3D Th–Co network of corner-sharing tetrahedra discernible after removal of the Sb atoms. Each tetrahedron is made by a central Co atom surrounded by four Th atoms.

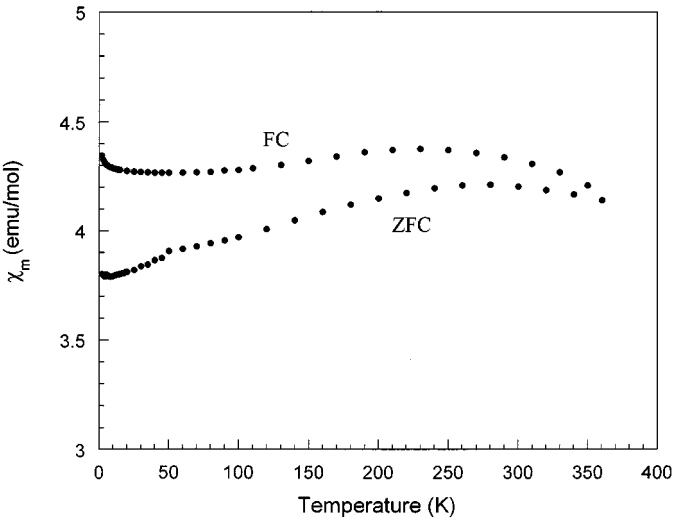

FIG. 4. Molar magnetic susceptibility curves (χ_m) for $Th_3Co_3Sb_4$ obtained under field-cooled (FC) and zero-filled-cooled (ZFC) conditions.

Crystal Structure Description

$Th_3Co_3Sb_4$ adopts the cubic space group *I*-43*d* (No. 220) and the $Y_3Au_3Sb_4$ structure type. This crystal structure can be viewed as a stuffed version of the Th_3Sb_4 structure (Th_3P_4 structure type) in which the Co atoms occupy the remaining empty tetrahedral sites corresponding to the 12b Wyckoff position. This complex dense three-dimensional structure does not allow a straightforward description, see Fig. 1. Note that cobalt bonds have been removed for clarity to emphasize the Th_3Sb_4 network in the figure. Two interpenetrated Sb tetrahedra surround the Th atoms, forming a pseudo-dodecahedron or more precisely a bis-disphenoid. This environment generates sets of inequivalent Th–Sb bonds (each set is made of four bonds) at 3.3590(9) and 3.2680(8) Å, Fig. 2B. The Sb atom is six-coordinated with the Th atoms defining a distorted octahedra as suggested by the Th–Sb–Th angles, see Table 4 and Fig. 2A. The Co atoms are coordinated to four Sb atoms at 2·6577(5) Å with four Th atoms at a longer distance of 2.9309(6) Å, forming a square antiprism distorted along the $\bar{4}$ axis, Fig. 2C.

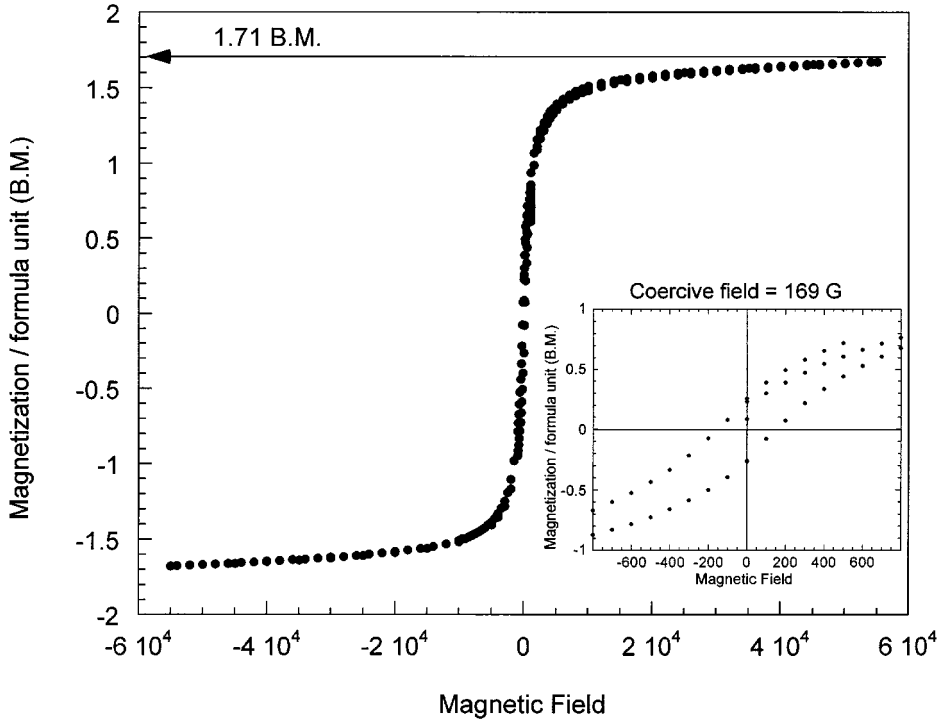

FIG. 5. Magnetization hysteresis loop for $Th_3Co_3Sb_4$ at 300 K.

In a description where the Sb atoms are removed from the structure, the Th atom is thus tetrahedrally surrounded by four Co atoms at 2.9309(6) Å. Each of these Co atoms is itself tetrahedrally coordinated with Th atoms to build a 3D framework of corner-sharing tetrahedra, see Fig. 3. The relatively short Th–Co distances could imply substantial bonding interactions between Th and Co and could explain some of the physical properties as discussed later in the electronic band structure and magnetism sections.

The observed bond distances of Th–Sb (3.3590(9) Å; 3.2680(8) Å) are in the same range as those observed in the binary compounds Th_3Sb_4 and $ThSb_2$ (37). The Co–Sb distance (2.6577(5) Å) is slightly longer than that in $CoSb_3$ (38) and CoSb (39) (2.5287 Å). However, the Th–Co bond lengths of 2.9309(6) Å are in fact shorter than those in ThCo and Th_2Co_{17} (40), where the mean bond distance is 3.1 Å. They are also shorter than the sum of the Van der Waals radii of the elements (3.05 Å).

Magnetism

The magnetic properties of $Th_3Co_3Sb_4$ were studied as a function of temperature. The magnetic susceptibility curves show evidence of long-range magnetic ordering below 300 K, as shown in Fig. 4. These curves are characteristic of a ferromagnetic compound even though the Curie temperature lies above the range of our data set. To further prove the ferromagnetic state, the magnetic hysteresis was measured at 2 and 300 K. The magnetization data at 300 K are shown in Fig. 5. The data obtained at 300 K are very similar to those at 2 K (except that the "knee" in the hysteresis loop is sharper and complete saturation is achieved almost immediately after), which suggests T_C lies consider-

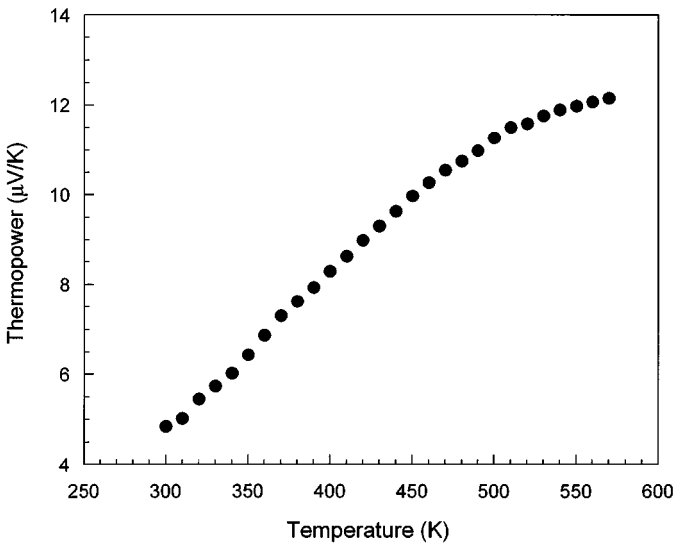

FIG. 6. Thermopower as a function of temperature for $Th_3Co_3Sb_4$.

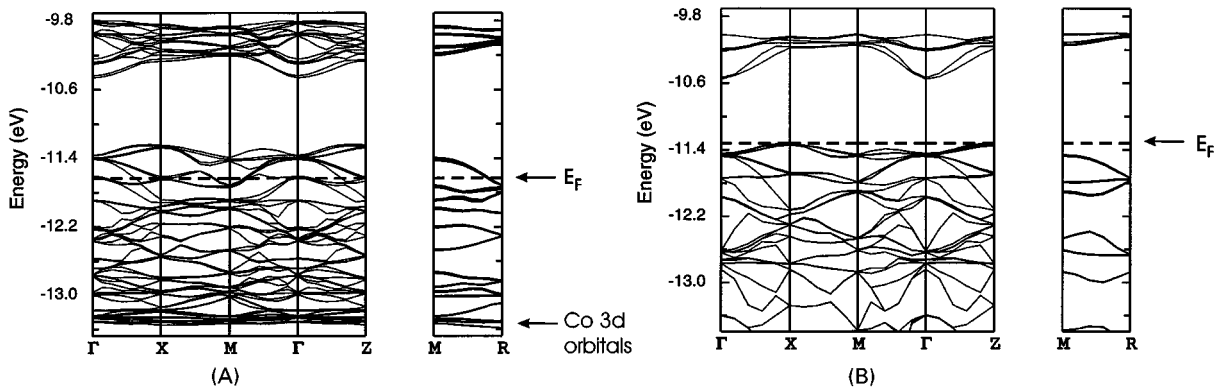

FIG. 7. Electronic band structure of (A) $Th_3Co_3Sb_4$ and (B) Th_3Sb_4. The Fermi level (E_F) is shown by the dashed line.

ably higher than room temperature. The magnetic hysteresis loop exhibits very sharp transitions typical of a strong ferromagnet. Saturation of the magnetic moment occurs at a field of $\sim 6 \times 10^4$ G. The corresponding effective magnetic moment is 1.71 B.M. per formula unit and 0.99 B.M. per Co atom. The calculated effective magnetic moment for Co in a neutral state is 1.72 B.M. This low-effective moment could be due to itinerant electrons arising from the strong hybridization of the Co 3*d* orbitals with the Sb and Th orbitals as discussed below. Although the measurements were performed well below the ordering temperature, the area enclosed by the hysteresis loop is very small, see inset Fig. 5. This reflects that $Th_3Co_3Sb_4$ possesses a small coercive field of 169 G. Consequently $Th_3Co_3Sb_4$ can be characterized as a soft but strong ferromagnet at room temperature.

Th ferromagnetic behavior suggests the presence of one type of magnetic moment, which by deduction is held by Co, assuming that Th^{+4} and Sb^{-3} possess no unpaired electrons. Considering that the ferromagnetic ordering occurs below the Curie temperature, $Th_3Co_3Sb_4$ should be a magnet at room temperature. Indeed, the compound is attracted to a permanent magnet.

Charge Transport Properties

As shown in Fig. 6, the thermopower increases as a function of increasing temperature. The room temperature value is low, $+5\ \mu V/K$, and rises up to $+13\ \mu V/K$ at 575 K. This positive and small Seebeck coefficient indicates that the compound is a *p*-type metallic conductor. The room temperature electrical conductivity was ~ 3800 S/cm, which is consistent with the metallic behavior. These properties are in agreement with the electrical behavior predicted from the electronic band structure calculations (see below). For comparison, the isostructural compound Th_3Sb_4 is an *n*-type semimetal (41) and shows a thermopower of $-52\ \mu V/K$ and an electrical conductivity of 3.08×10^{-4} S/cm at room temperature (42). Clearly, in this case the insertion of Co within the Th–Sb framework is responsible in transforming the material from semiconductor to metal.

Electronic Structure

In order to prove the role of Co on the physical properties of $Th_3Co_3Sb_4$, electronic band structure calculations were performed on both $Th_3Co_3Sb_4$ and Th_3Sb_4. A comparison between the two band structures provides better insights regarding the bonding and charge distribution within the compound. The extended Hückel method despite its limitations gave a satisfactory result in a way that is consistent with those obtained earlier on Th_3Sb_4 and $Th_3Ni_3Sb_4$ (24), using more elaborate methods such as the self-consistent APW method.

At first glance, if we ignore the Co 3*d* orbitals, both calculated electronic structures show similar features as shown in Fig. 7. Th_3Sb_4 appears as a semiconductor with an indirect energy gap, whereas $Th_3Co_3Sb_4$ is a metal in agreement with the experimental data discussed above. A set of weakly dispersed bands lying at the ionization potential of the Co 3*d* (in the neighborhood of -13.5 eV) has essentially Co 3*d* character hybridized over 20% with Th 5*f*, 6*d*, 7*p*, and is weakly hybridized with Sb 5*p* orbitals, see density of states (DOS) in Fig. 8A. This strong mixing between the Th 6*d*, 5*f*, and Co 3*d* orbitals raise the bottom of the Th 6*d*, 5*f*, bands, compared to those in Th_3Sb_4, Fig. 8. Co 3*d* and Sb 5*p* states are less strongly mixed; the spike of Co 3*d* density of states at -13.3 eV lies on a minimum of Sb 5*p* DOS. Therefore the bottom of the Sb bands is slightly raised in $Th_3Co_3Sb_4$, giving rise to the metallic and possibly ferromagnetic properties. The low value of the effective magnetic moment may be due to itinerant electrons within the hybridized Co–Th orbitals. Between the Fermi level and -16 eV and without considering the Co 3*d* orbitals, a broad set of very dispersed bands is largely dominated by an almost equal contribution of Th 6*d*, 5*f*, and Sb 5*p* orbitals, giving rise to strong Sb–Th interactions, see Fig. 8A. This is

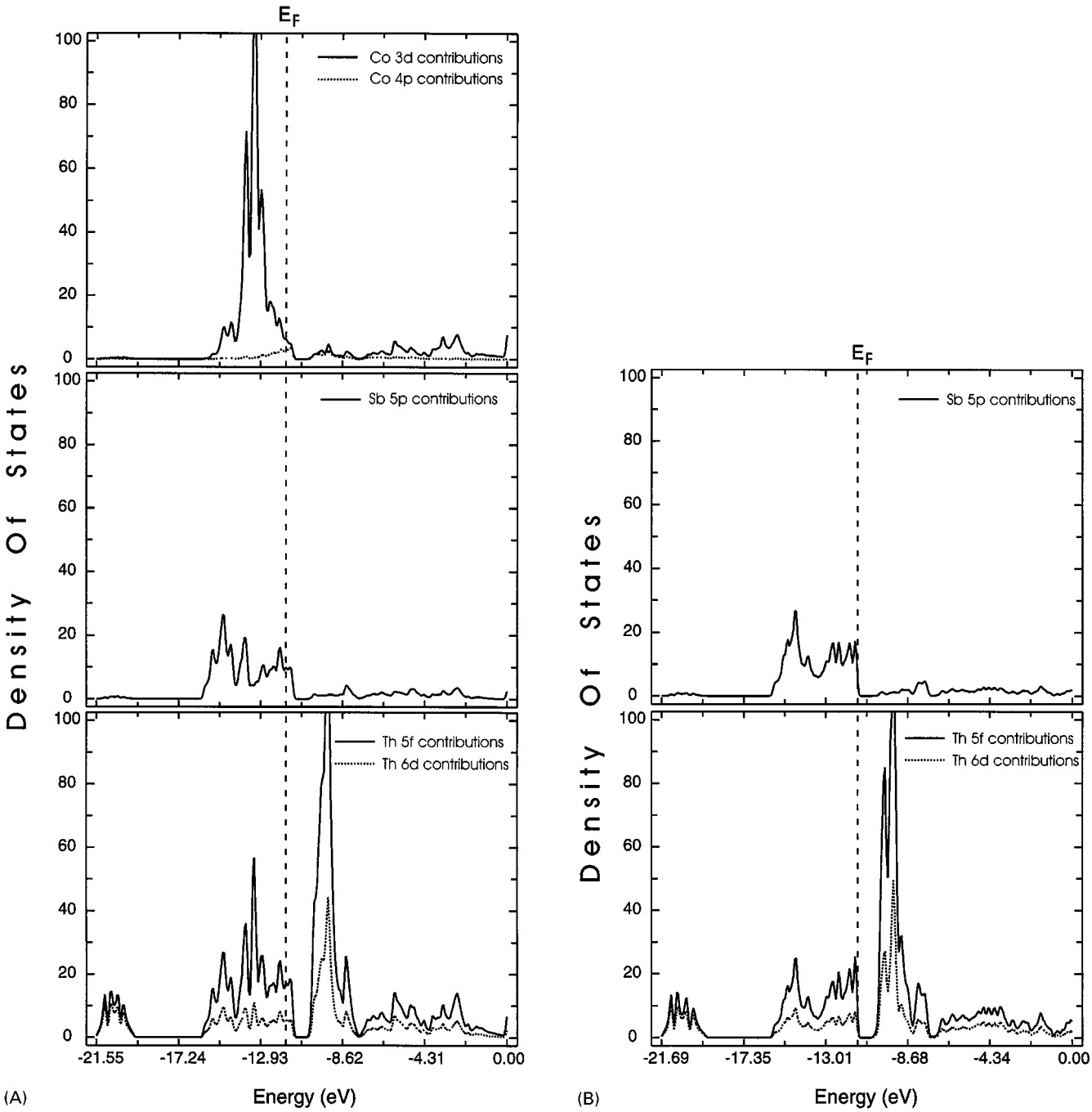

FIG. 8. Partial DOS plots for $Th_3Co_3Sb_4$ and Th_3Sb_4. (A) Contribution to the DOS of Sb 5*p*, Th 6*d*, 5*f*, and Co 3*d*, 4*p* for $Th_3Co_3Sb_4$. (B) Contribution to the DOS of Sb 5*p*, and Th 6*d*, 5*f* for Th_3Sb_4. The Fermi level is shown by the dashed line.

not surprising since the weakly contracted 5*f* shell is expected to strongly mix its valence orbitals with those of the neighboring atoms. Above the Fermi level, the bands for both compounds consist primarily of empty Th 5*f*, 6*d*, and 7*p* orbital mixture, see DOS Fig. 8A. The hybridization character can be described as 65.5% *f*, 20% *d*, 14% *p*, and 0.5% of both Sb *p* and Co *p*. Overall, the main contributions of the Th orbitals are localized above the Fermi level, confirming an oxidized state on the Th atoms of +4.

One of the questions raised in $Th_3Co_3Sb_4$ is the nature of the metal–metal (Th–Co) interaction. Bonding insight is gained by the analysis of the crystal orbital overlap popula-

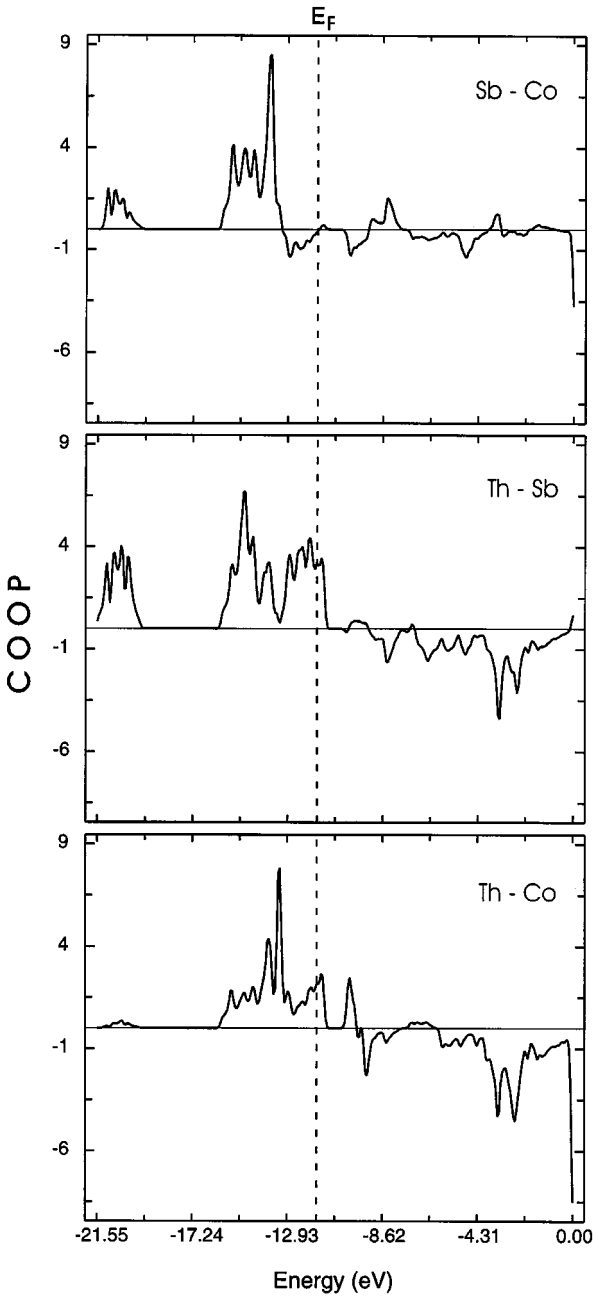

FIG. 9. COOP curves for $Th_3Co_3Sb_4$ corresponding to Sb–Co, Th–Sb, and Th–Co bonds. The Fermi level is shown by the dashed line. Positive COOP numbers on the *y* axes indicate bonding levels, and negative numbers indicate antibonding levels.

tion (COOP) using Th–Sb COOP from Th_3Sb_4 as a reference to assess the bond strength. The nature of the Th–Sb bond is not significantly different in both compounds. The corresponding Fermi levels are located below antibonding levels and the observed Mulliken overlap populations (MOP) are similar at 0.35 and 0.434 for $Th_3Co_3Sb_4$ and Th_3Sb_4, respectively. COOP for Th–Co interactions are bonding with a substantial MOP of 0.18 and the Fermi level is located below the antibonding levels, see Fig. 9. In contrast, for COOP corresponding to Sb–Co interactions some antibonding levels are filled below the Fermi level, which lies on a slightly antibonding minimum. However, the overall MOP is bonding with a significant population of 0.18. Given that the Th–Co distance is relatively short and the fact that only bonding levels are populated with a significant MOP imply strong Th–Co bonding interactions. Therefore, contrary to what is expected, Co–Sb bonds are weaker than those of Th–Co. All bonds, Th–Co, Th–Sb, and Co–Sb, possess a strong covalent character, which is responsible for the compound formation, and ensure the cohesion of the 3D network.

Attempts to assign formal charges based on localized Mulliken populations would be unrealistic since the actinides do not possess a localized 5*f* shell. However, it seems reasonable to use the analogy with Th_3Sb_4 and $Th_3Ni_3Sb_4$ (24) associated with the Pauling's electronegativity and the fact that Th is very electropositive and probably fully oxidized. In this context we propose the formalism $(Th^{+4})_3(Co^0)_3(Sb^{-3})_4$. Such a description is in agreement with the density of states. Since the calculations suggest that the Co 3*d* orbitals are not completely filled, an oxidation state slightly higher than 0 (i.e., $+\delta$) seems plausible. This assignment is supported by the measured magnetic moment which seems to derive only from Co.

CONCLUDING REMARKS

A new metallic ferromagnetic compound $Th_3Co_3Sb_4$ with $T_c \gg 300$ K was discovered with the $Y_3Au_3Sb_4$ structure type. The electronic band structure calculations show the importance of Th–Co bonding interactions on its physical properties. The metallic behavior arises from hybridization of the Co 3*d* orbitals with the Th 6*d*, 5*f* orbitals, whereas the magnetic moment is believed to come from a formally neutral Co.

ACKNOWLEDGMENT

Financial support from the Department of Energy is gratefully acknowledged.

REFERENCES

1. A. E. Dwight, *Acta Crystallogr. Sect. B* **33,** 1579–1581 (1977).
2. M. Wang, R. McDonald, and A. Mar, *Inorg. Chem.* **38,** 3435–3438 (1991).
3. M. Kasaya, K. Katoh, and K. Takegahara, *Solid State Commun.* **78,** 797–800 (1991).
4. K. Katoh and M. Kasaya, *Physica B* **188,** 428–430 (1993).
5. K. Katoh and M. Kasaya, *J. Phys. Soc. Jpn.* **65,** 3654–3660 (1996).
6. D. Young, K. Mastronardi, P. Khalifah, C.-C. Wang, R. J. Cava, *Appl. Phys. Lett.* **74,** 3999–4001 (1999).

7. T. Endstra, G. J. Nieuwenhuys, J. A. Mydosh, and K. H. J. Buschow, *J. Magn. Magn. Mater.* **89,** L273–L276 (1990).
8. A. E. Dwight, *J. Nucl. Mater.* **79,** 417 (1979).
9. K. H. J. Buschow, D. B. Mooij, T. T. M. Palstra, O. J. Nieuwenhuys, and J. A. Mydosh, *Philips J. Res.* **40,** 313–322 (1985).
10. K. Takegahara and Y. Kaneta, *Prog. Theor. Phys. Suppl.* **108,** 55–71 (1992).
11. T. Takabatake, S.-I. Miyata, H. Fujii, Y. Aoki, T. Suzuki, T. Fujita, J. Sakurai, and Hiraoka, *J. Phys. Soc. Jpn.* **59,** 4412–4418 (1990).
12. R. V. Skolozdra, P. S. Salamakha, A. L. Ganzyuk, and O. I. Bodak, *Izv. Akad. Nauk. SSSR Neorg. Mater.* **29,** 25–27 (1993).
13. Z. Fisk, J. D. Thompson, and H. R. Ott, *J. Magn. Magn. Mater.* **76,** 637–641 (1988).
14. M. F. Hundley, A. Lacerda, P. C. Canfield, J. D. Thompson, and Z. Fisk, *Physica B* **186&188,** 425–427 (1993).
15. A. Severing, J. D. Thompson, P. C. Canfield, Z. Fisk, and P. Riseborough, *Phys. Rev. B* **44,** 6832–6837 (1991).
16. G. Aeppli and Z. Fisk, *Comments Condens. Matter Phys.* **16,** 155–165 (1992).
17. T. Takabatake, S.-I. Miyata, H. Fujii, Y. Aoki, T. Suzuki, and T. Fujita, *Physica B* **165,** 437–438 (1990).
18. S. Patil, Z. Hossain, P. L. Paulose, R. Nagarajan, L. C. Gupta, and C. Godart, *Solid State Commun.* **99,** 419–422 (1996).
19. G. A. Slack, *J. Phys. Chem. Solids* **34,** 321–335 (1973).
20. G. D. Mahan, *Solid State Phys.* **51,** 81–157 (1998).
21. K. Fess, W. Kaefer, Ch. Thurner, K. Friemelt, Ch. Kloc, and E. Bucher, *J. Appl. Phys.* **83,** 2568–2573 (1998).
22. C. D. W. Jones, K. A. Regan, and F. J. DiSalvo, *Phys. Rev. B* **58,** 16,057–16,063 (1998).
23. Y. Aoki, T. Suzuki, T. Fujita, T. Takabatake, S.-I. Miyata, and H. Fujii, *J. Phys. Soc. Jpn.* **61,** 684–691 (1992).
24. Y. Takegahara, Y. Kaneta, and T. Kasuya, *J. Phys. Soc. Jpn.* **59,** 4394–4404 (1990).
25. SMART: Siemens Analytical X-ray Systems, Inc., Madison, WI 53719, 1994.
26. SAINT: Version 4, Siemens Analytical X-ray Systems, Inc., Madison, WI 53719, 1994–1996.
27. G. M. Sheldrick, University of Göttingen, Germany, to be published.
28. SHELXTL: Version 5, G. M. Sheldrick, Siemens Analytical X-ray Systems, Inc., Madison, WI 53719, 1994.
29. P. W. Selwood, *in* "Magnetochemistry," 2nd ed. Interscience, New York, 1956.
30. M.-H. Whangbo and R. Hoffmann, *J. Am. Chem. Soc.* **100,** 6093–6098 (1978).
31. J. Ren, W. Liang, and M.-H. Whangbo, "Crystal and Electronic Structure analysis Using CAESAR." PrimeColor Software, Inc., NC, 1998.
32. H_{ii} values are taken from the CAESAR package data base.
33. R. H. Summerville and R. Hoffmann, *J. Am. Chem. Soc.* **98,** 7240–7254 (1976).
34. K. Tatsumi and A. Nakamura, *J. Am. Chem. Soc.* **109,** 3195–3206 (1987).
35. T. Hughbanks, R. Hoffmann, M.-H. Whangbo, K. R. Stewart, O. Eisenstein, and E. Canadell, *J. Am. Chem. Soc.* **104,** 3876–3879 (1982).
36. J. Ammeter, H.-B. Bürgi, J. Tibeault, and R. Hoffmann, *J. Am. Chem. Soc.* **100,** 3686–3692 (1978).
37. R. Ferro, *Acta Crystallogr.* **9,** 817–818 (1956).
38. Th. Schmidt, G. Kliche, and H. D. Lutz, *Acta Crystallogr. Sect. C* **43,** 1678–1679 (1987).
39. A. Kjekshus and K. P. Walseth, *Acta Chem. Scandinavica* **23,** 2621–2630 (1969).
40. J. V. Florio, N. C. Baenziger, and R. E. Rundle, *Acta Crystallogr.* **9,** 367–372 (1956).
41. Z. Henkie and C. Bazan, *Phys. Stat. Sol. A* **5,** 259–268 (1971).
42. C. E. Price and I. H. Warren, *J. Electrochem. Soc.* **112,** 510–513 (1965).